ROYAL SOCIETY
OF CHEMISTRY

PAPER

Check for updates

A family of luminescent metal–organic frameworks: synthesis, structure, and sensing studies†

Hariprasad Pulijala,[a] Tentu Nageswara Rao, [iD][b] Faheem Ahmed[c] and Y. Prashanthi*[a]

Herein we report three novel luminescent metal–organic frameworks (MOFs) *viz.* $[Co(bpeb)(hfipbb)_{0.5}]_n$ (**LCo-1**), $[Zn(bpeb)_2(hfipbb)]_n$ (**L-Zn**) and $[Co(bpeb)_2(oba)]_n$ (**LCo-2**) (where bpeb, hfipbb and oba represent (1,4-bis[2-(4-pyridyl)ethynyl]benzene), 4,4′-(hexafluoroisopropylidene)bis(benzoic acid) and $4,4^1$-oxybis(benzoic acid) respectively), which were synthesized through the solvothermal method and characterized by SC-XRD. Compounds **LCo-1** and **L-Zn** adopt two-dimensional layered structures while compound **LCo-2** is a 3-dimensional framework. The observed dimensionality changes of **LCo-1** and **LCo-2** from 2D to 3D are due to the different bridging modes of carboxylic acid ligands. In **LCo-1** and **L-Zn**, the hfipbb ligand coordinates to the metal center in a monodentate fashion $\{(\kappa^1)-(\kappa^1)-(\kappa^1)-(\kappa^1)-\mu_4\}$, and in **LCo-2**, dba coordinates in a $\{(\kappa^1)-(\kappa^1)-\mu_2\}$ manner. Photoluminescence studies reveal that all three compounds show interesting sensing behavior towards nitroaromatic compounds.

Introduction

Over the last two decades, metal–organic frameworks (MOFs) have received extensive attention due to their interesting structure-related properties and endless number of possible structures.[1–4] MOFs are well studied for their potential in gas storage and separation,[5] catalysis,[6,7] luminescence,[8] molecular magnetism[9] and various other properties.[10] In this context, MOFs with luminescence properties have attracted considerable attention in sensing organic molecules and metal ions.[11–15] Selective detection of nitro explosives using MOFs is attracting immense attention owing to their variety of potential applications in security operations, forensic investigations and mine-field analysis.[16–20] Luminescent MOFs made by using flexible ligands to synthesize soft and guest responsive MOF probes in the detection of organic molecules at ultra-trace levels have been focused on more.[21–23] Unlike rigid MOFs, the conformational orientations according to the size of the guest entity are adjustable with flexible MOFs.[24]

Luminescent MOFs for the detection of nitroaromatic compounds are important in addressing global issues like pollution control and present-day security control.[25–28] These nitroaromatic compounds are derivatives or reactants of dyes, pesticides, and pharmaceutical industries, and molecules such as 2,4,6-trinitrotoluene (TNT), 2-nitrophenol (2NP), 4-nitrophenol (4NP), and 2,4,6-trinitrophenol (TNP) are used for making explosives and are considered as hazardous to health even when present in a trace quantity.[29,30] Herein, our work aims to synthesize novel Co and Zn-based flexible luminescent MOFs that are effective for the detection of nitroaromatic compounds at an ultra-trace level. MOFs with flexible ligands with free C–C rotation for conformational freedom have been focused on. These MOFs form 2D- and 3D-structures *via* bridge bonds by the ligands with metal atoms. The bidentate ligands, such as bpeb, and tetradentate ligands such as hfipbb and oba are employed as coordinating molecules to the central metal atoms (Zn and Co) to form pyridinyl and carboxylic linkages respectively. The molecular formulae of the as-synthesized MOFs are $[Co(bpeb)(hfipbb)_{0.5}]_n$ (**LCo-1**), $[Zn(bpeb)_2(hfipbb)]_n$ (**L-Zn**) and $[Co(bpeb)_2(oba)]_n$ (**LCo-2**).

[a] *Department of Chemistry and Pharmaceutical Sciences, Mahatma Gandhi University, Nalgonda, Telangana, 508001, India. E-mail: prashanthimgu@gmail.com*

[b] *Department of Chemistry, Krishna University, Machilipatnam Andhra Pradesh 521001, India*

[c] *Department of Physics, College of Science, King Faisal University, Hofuf Al-Ahsa 31982, Saudi Arabia*

† Electronic supplementary information (ESI) available. See DOI: 10.1039/d0ma00889c

Experimental

Synthesis of $[Co(bpeb)(hfipbb)_{0.5}]_n$ (LCo-1)

(1,4-Bis[2-(4-pyridyl)ethynyl]benzene) (bpeb) is synthesized by the literature method.[31] A mixture containing $Co(NO_3)_2 \cdot 6H_2O$

(41.4 mg, 0.14 mmol), hfipbb (40 mg, 0.1 mmol), and bpeb (40.4 mg, 0.14 mmol) dissolved in H_2O (3 ml), DMF (3 ml), and DMSO (2 ml) was placed in a 15 ml pressure tube and then 10 drops of NaOH (0.1 M) solution were added. The tube was properly sealed and kept at 150 °C for 12 h. After cooling down the tube to room temperature, yellow-colored X-ray quality crystals of **L-Co** were obtained at the bottom of the tube (yield = 20% based on metal). FT-IR (KBr pellet, cm^{-1}): 3411(br), 3169(w), 1631(m), 1583(w), 1433(s), 1058(br).

Synthesis of $[Zn(bpeb)_2(hfipbb)]_n$ (L-Zn)

LZn-1 is synthesized by using the same technique applied for **LCo-1** by replacing the metal source by $Zn(NO_3)_2 \cdot 6H_2O$ (0.14 mmol) in place of $Co(NO_3)_2 \cdot 6H_2O$, and using hfipbb (0.2 mmol) and bpeb (0.28 mmol) as coordinating ligands. Yield (33% based on nickel). Elemental analysis. Anal. calc. data: C, 35.1%; H, 4.5%; N, 4.8%; S, 11.0%. Found: C, 34.5%; H, 4.1%; N, 4.1%; S, 10.5%. FT-IR (KBr pellet cm^{-1}) 3440(br), 1590(s), 1480(w), 1401(s), 1324(w), 1213(m), 1102(br).

Synthesis of $[Co(bpeb)_2(oba)]_n$ (LCo-2)

The same technique as followed for **LCo-1** was employed for the synthesis of **LCo-2** using $Co(NO_3)_2 \cdot 6H_2O$ as the metal precursor and bpeb (0.28 mmol) and oba (0.2 mmol) as organic linkers. Yield (31% based on cobalt). Elemental analysis. Anal. calc. data: C, 45.5%; H, 2.8%; N, 7.0%; S, 16.2%. Found: C, 44.9%; H, 2.4%; N, 6.4%; S, 15.5%. FT-IR (KBr pellet cm^{-1}) 3424(br), 1636(m), 1607(s), 1434(s), 1309(w), 1239(w), 1009(w).

Characterization

On a PerkinElmer TGA 4000 instrument, the thermogravimetric analysis was performed. The IR spectra of compounds 1–3 were recorded on a PerkinElmer FT-IR Spectrum BX using KBr pellets in the 4000–400 cm^{-1} region. Elemental analysis was performed on an ElementalMicro Vario Cube Elemental Analyzer. PXRD patterns were measured on a Panalytical EMPYRIAN instrument using Cu Ka radiation. Single crystal data for compounds were collected on a Bruker SMART diffractometer equipped with a graphite monochromator and Mo-Ka (a = 0.71073 Å, 296 K) radiation. Collection of data were carried out using Δ and a scans. Structures were resolved using direct methods followed by a full matrix with the least square F^2 refining (all HKLF^4 data format) using SHELXTL. The positions of the remaining non-hydrogen atoms were revealed by subsequent differences in Fourier synthesis and least-square refinement. According to the established procedures, determination of the crystal system, orientation matrix, and cell dimensions was conducted. Lorentz polarization and correction of multi-scan absorption were applied. With independent anisotropic displacement parameters, non-hydrogen atoms were refined and hydrogen atoms were placed geometrically and refined using the riding model. All calculations were carried out using SHELXL 97,20 PLATON 99 and WinGXsystemVer-1.64. Since compound 1 contains a solvent-accessible void, the SQUEEZE program was applied and details of the squeezed material from the SQF file

are included in the final.CIF file for synthesized compounds. Data collection and structure refinement parameters and crystallographic data for compounds 1–3 are given in Table 1. Selected bond lengths and bond angles for compounds 1–3 are given in Table S1 (ESI†).

Results and discussion

The molecular structures of ligands bpeb, hfipbb, and dba are shown in Scheme 1; the pyridinyl ligand bpeb can coordinate to the central atom in a bidentate manner, whereas the carboxylic ligands hfipbb and oba can coordinate in a tetradentate manner. Typical MOF synthesis procedures are shown in Scheme 2; the colored precipitate formation after completion of the reaction is noticed in each MOF synthesis. The single-crystal X-ray diffraction analysis of these MOFs reveals that all MOFs (**LCo-1**, **L-Zn**, and **LCo-2**) crystallize in a structure with $P2/c$ symmetry (Table 1). Further close examination of each individual MOF reveals that though they acquire similar crystalline structures, the bonding environment, the structural orientation, reactive void size, and extended polymer structures are unique to each other.

### Structural description of $[Co(bpeb)(hfipbb)_{0.5}]_n$ (LCo-1)

The X-ray diffraction results and the thermal stability of **LCo-1** are shown in Fig. 1. The asymmetric unit of the **LCo-1** MOF showed that the central metal atom (Co1) acquired the distorted octahedral structure (Fig. 1(a)) and the coordination environment contains four carboxylate oxygen atoms (O1) of four different hfipbb ligands in axial positions by O1–Co1–O1 linkages and with one pyridine ring of bpeb equatorially with a Co–N linkage, and a single bpeb ligand holds two Co atoms at a time. The (hfipbb) ligands hold four Co(II) centers in a monodentate fashion $\{(\kappa^1)-(\kappa^1)-(\kappa^1)-\mu_4\}$ leaving the remaining oxygen atoms to extend the coordination in the c-direction to form a 2d-MOF network by bridging four Co centers (Fig. 1(b) and (c)). The (O–Co–O) bond distances are in the range of 2.025–2.102 Å, the Co–N bond distance is 2.054 Å, the (O–Co–O) bond angles around the Co(II) center are in the range of 87.32(1)–91.61(1)°, and the (N–Co–O) bond angles are in the range of 91.94(4)–104.44(6)° (Table S1, ESI†). On the other hand the bpeb linkers hold two Co centers; each Co(II) center bridged by bpeb extended its structure in either the a or b-direction (Fig. 1(c)) to form two independent 1D chains. It is worth mentioning that these independent chains are stitched by hfipbb ligands to form a 2D sheet in the ab-plane (Fig. 1c). Careful analysis reveals that each bpeb bridged 1D chain is crisscrossed over one another *i.e.* arranged on the top and bottom of the plane containing hfipbb ligands and Co(II) centres as shown in Fig. 1(c). PLATON analysis reveals ~39% pore accessible void volume (4033.4 Å^3 per unit cell volume 10383.0 Å^3) in **L-Co**. It can be seen that a basic unit, $[Co(bpeb)(hfipbb)_{0.5}]$, is repeated to form a complete 2D sheet and hence can be termed as the Secondary Building Unit (SBU), where each SBU is connected to eight neighboring SBUs by the hfipbb ligand and two SBUs by bpeb linkers to form the

Table 1 Crystallographic data parameters for the as-synthesized compounds **L-Co**, **LZn-1**, and **LCo-2**

Parameter	LCo-1	L-Zn	LCo-2
Empirical formula	$(C_{54}H_{32}N_2O_8F_{12}Co_2)_n$	$(C_{54}H_{32}N_2O_8F_{12}Zn_2)_n \cdot H_2O_2$	$(C_{48}H_{32}N_2O_{10}Co_2)_n \cdot 3(H_2O_1)$
CCDC number	997056	997058	997055
Formula weight	591.339408	614.81	962.62
Crystal shape	Block	Block	Block
Color	Pink	Yellow	Pink
Size (mm)	0.42 × 0.36 × 0.28	0.42 × 0.35 × 0.28	0.46 × 0.35 × 0.30
Crystal system	Monoclinic	Monoclinic	Monoclinic
Space group	$P2/c$	$P2/c$	$P2_1/c$
a/Å	15.6195(12)	15.6221(5)	13.8008(15)
b/Å	8.1665(6)	8.2361(3)	24.780(3)
c/Å	22.8034(18)	22.6803(8)	16.5096(17)
α (°)	90.0	90.0	90.0
β (°)	104.063(4)	104.149(2)	115.575(7)
γ (°)	90.0	90.0	90.00
Cell volume V (Å^3)	2821.5(4)	2829.67(17)	5092.82(10)
Cell formula units Z	4	4	2
Density (g cm^{-3})	1.392 g cm^3	1.443 g cm^3	1.255 g cm^3
μ (mm)	0.678	0.943	0.704
Wavelength (Mo kα) (Å)	0.71073	0.71073	0.71073
Temperature (K)	296(2)	296(2)	296(2)
Theta range for data collection	2.49–21.87	5.43–25.85	5.13–24.47
Total reflections	6458	6742	12819
Unique reflections	6453	5175	7648
$F(000)$	1192	1240	1968
R_{factor} all^a	0.0714	0.0647	0.1151
wR_2^{b}	0.2256	0.1626	0.2393
Goodness-of-fit	1.099	1.035	1.093

^{a} $R_1 = \Sigma \|F_o| - |F_c\|/\Sigma|F_o|$. ^{b} $R_2 = [\Sigma\{w(F_o^2 - F_c^2)^2\}/\Sigma\{w(F_o^2)^2\}]^{1/2}$.
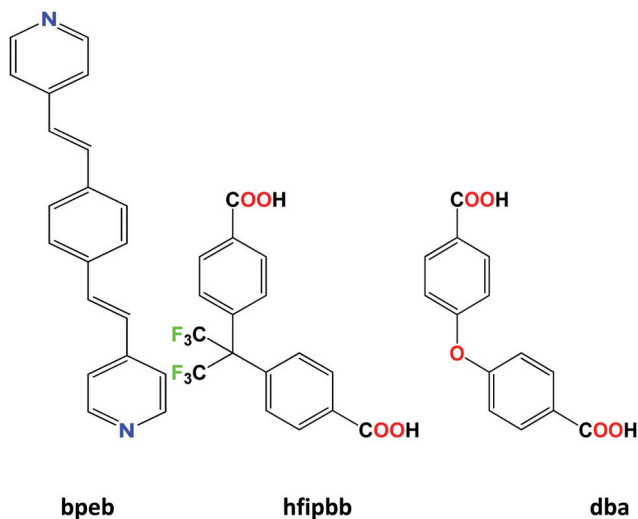
Scheme 1 Ligands used for the present work.

extended structure. Fig. 1(d) shows thermogravimetric analysis (TGA) of **LCo-1**. It is observed that the compound showed thermal stability up to 295 °C and after that continuous weight loss is observed with the increase of temperature; this change may be attributed to the combustion of organic matter in the presence of air at higher temperature.

### Structural description of [Zn(bpeb)$_2$(hfipbb)]$_n$ (L-Zn)

The asymmetric unit of **L-Zn** consists of Zn(II) as a central metal atom with four oxygen atoms of hfipbb as the coordinating

ligand from the axial direction ({(κ^1)-(κ^1)-(κ^1)-(κ^1)-μ$_4$} fashion) and the pyridine linkage of the bpeb equatorial position (Fig. 2(a) and (b)). The coordinated hfipbb ligands for Zn(II) are *trans* to each other and the (O–Zn–O) bond distances are in the range of 2.031–2.073 Å, the Zn–N bond distance is 2.017 Å, the (O–ZN–O) bond angles around the Zn(II) centers are in the range of 87.36(6)–90.24(0)° and the (N–Zn–O) bond angle is 96.35(1)–104.04(8)° (Table S1, ESI†). hfipbb extends its bonding to another eight Zn centers in the *c*-direction, whereas the bpeb linker coordinates Zn(II) from the top and the linkage extends for other Zn(II) to acquire the 2d-structure in *a*- or *b*-directions (Fig. 2(c)). PLATON analysis reveals no solvent accessible area in the 2D framework. However, the desolated framework contains ∼39% pore accessible void volume (1904.7 Å^3 per unit cell volume 4897.1 Å^3). The TGA curve of the corresponding **L-Zn** showed thermal stability up to 295 °C.

Structural description of [Co(bpeb)$_2$(oba)]$_n$ (LCo-2)

Though **LCo-2** crystallizes in the monoclinic system with $P2_1/c$ space group similar to **LCo-1**, the asymmetric center (Co(II)) acquires a distorted octahedral structure and the coordinating environment contains the bpeb ligand which is coordinated to the central metal atom equatorially and three oba linkers from the axial position (Fig. 3(a) and (b)). In contrast to compounds **L-Co** and **L-Zn**, in **LCo-2** three out of four oba ligands coordinate Co(II) centers in a monodentate bridging mode {(κ^1)-(κ^1)-(κ^1)-(κ^1)-μ$_4$} by O–C–O linkage and the remaining one dba molecule coordinates in a bidentate mode {(κ^1)-(κ^1)-μ$_2$} (Fig. 3(a)–(c)). Co1–O is in the range of 2.0051–2.206 Å, the (Co1–N) bond distance is 2.1119 Å, Co2–O is in the range of 1.944–2.4324 Å,
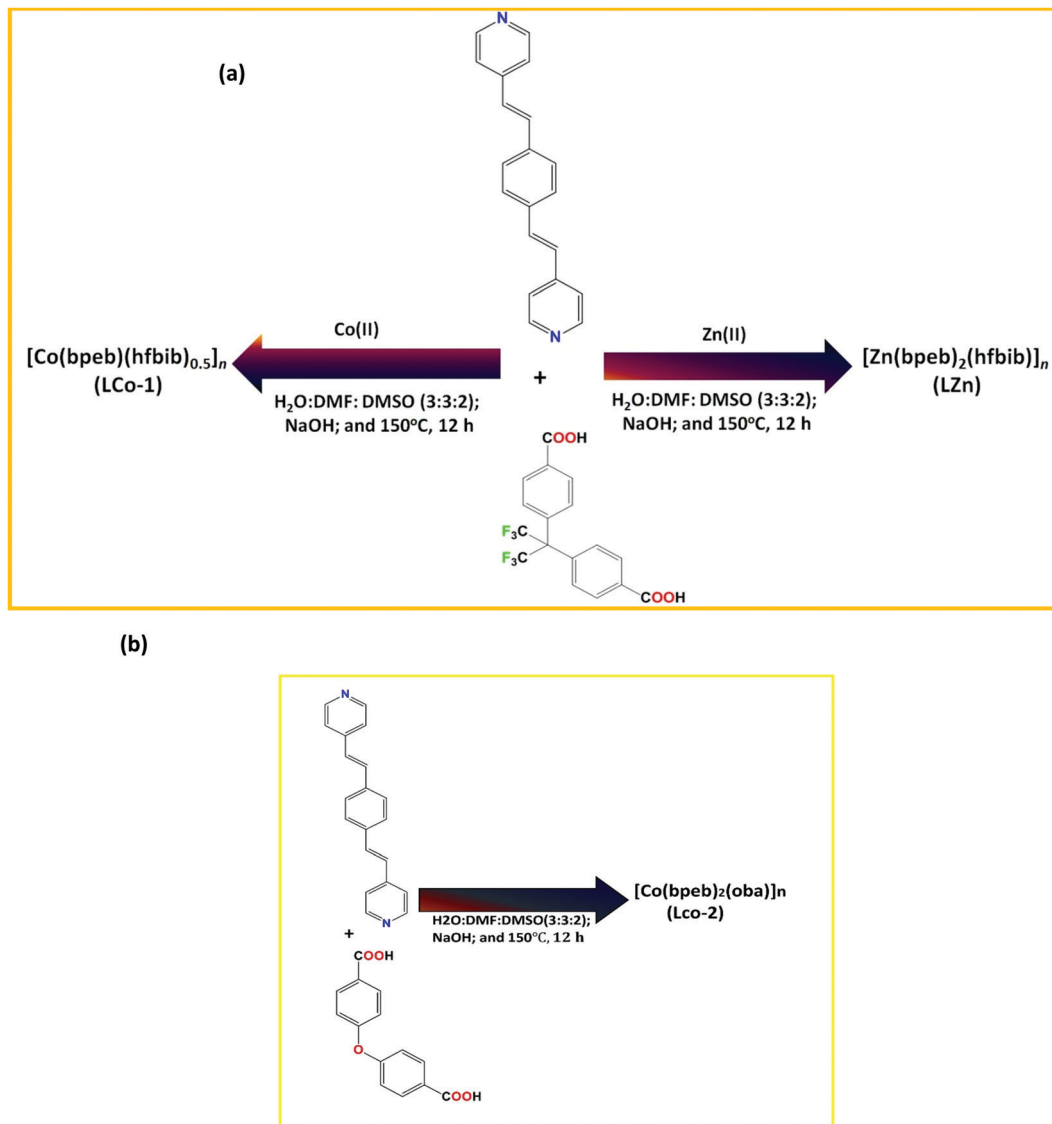
Scheme 2 Synthetic details of compounds (a) **LCo-1** and **L-Zn**; and (b) **LCo-2**.

and the (Co2–N) bond distance is 2.0374 Å (Table S1, ESI†). Ligands bpeb and dba extend their bonding to other Co centers, and the bridging mode bpeb ligands extend their 1D chains along the *ac*-plane to form 3D-structures. Similarly, the dba ligands extend the bonding in the *a*- and *b*-direction. As the oba ligand is a structurally bent-shape, it plays a crucial role in making the structure three dimensional. PLATON analysis reveals no solvent accessible area in the 2D layer. However, the desolated framework contains only ~9% pore accessible void volume (135.5 Å^3 per unit cell volume 1582.6 Å^3). The arrangements of bpeb ligands in the channels are favored by the weak C–H···π (3.470(6) Å) and C–H···O interactions (3.239(6)–3.473(6) Å) respectively. The TGA curve of the corresponding **L-Co-2** showed thermal stability up to 365 °C.

It can be seen that one basic unit [Co(bpeb)$_2$(oba)]$_n$ is repeated to form the complete framework and hence this unit is termed as the SBU for **LCo-1**.

Fig. 4(a) shows the photoluminescence (PL) spectra of the synthesized compounds. The π-electron-rich environment in the MOF structure made the compounds efficient for exhibiting luminescence properties. The PL spectra of **LCo-1** and **L-Zn** dispersed in DMF exhibit strong fluorescence bands at 413 nm and 414 nm respectively upon excitation of compounds at 340 nm and these emission bands are attributed to the ligand to metal charge transfer (LMCT) effect within the MOF structure. Along with the LMCT peaks, the shoulder peaks for **LCo-1** and **L-Zn** are observed at 391 nm and 392 nm respectively; these bands are attributed to the ligand charge transitions (LLCT) between free bpeb and coordinated bpeb ligands. Similar peaks are also observed for **LCo-2** at 411 nm and 391 nm of LMCT and LLCT respectively (Table S2, ESI†). The sensing ability of the as-synthesized compounds towards different nitroaromatic compounds is shown in Fig. 4 and 5. The fluorescence intensity quenching ability of nitroaromatic compounds as a function of
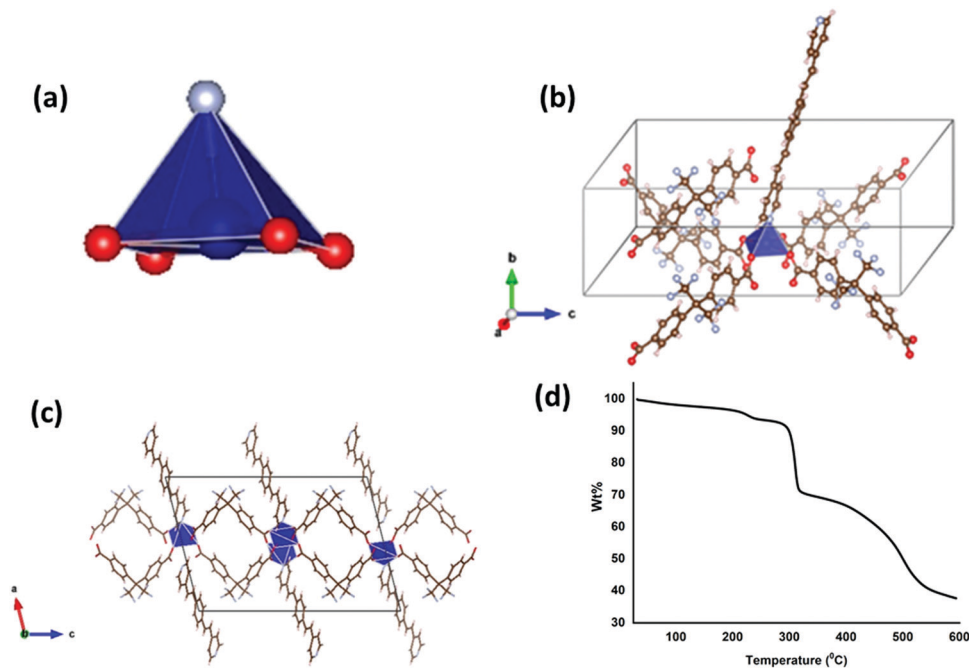
Fig. 1 (a) The SBU unit of the **LCo-1** MOF with color code blue: central atom (Co), red: oxygen atoms and indigo blue: nitrogen; (b) complete structure of the SBU with coordinating molecules (bpeb and hfipbb); (c) 2-dimensional structure; and (d) thermogravimetric curve of the **LCo-1** MOF.
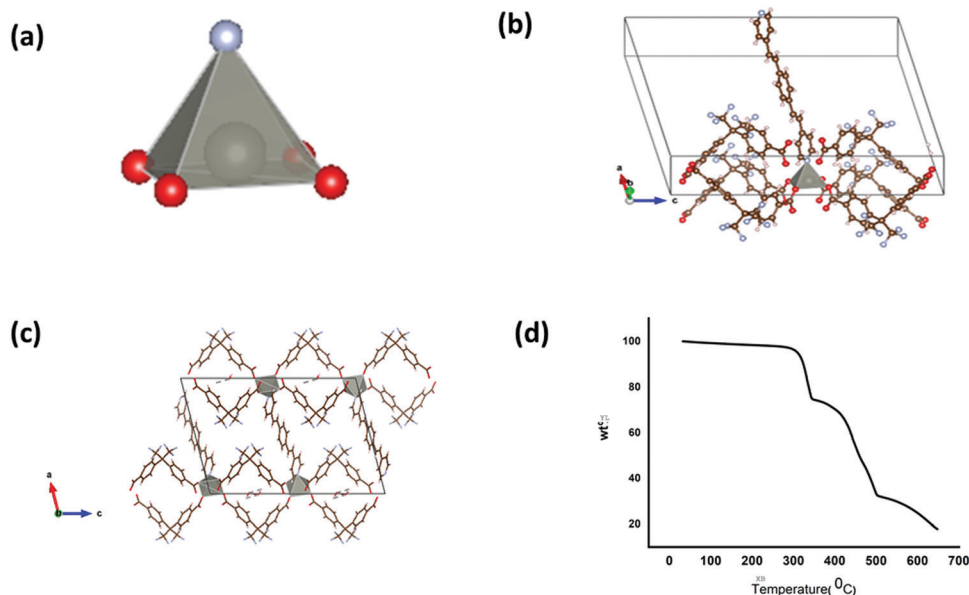

Fig. 2 (a) The SBU unit of the **L-Zn** MOF with color code black: central atom (Zn), red: oxygen atoms and indigo blue: nitrogen; (b) complete structure of the SBU with coordinating molecules (bpeb and hfipbb); (c) 2-dimensional structure; and (d) thermogravimetric curve of the **L-Zn** MOF.

analyte concentration is plotted (Fig. 4). The efficiency of **LCo-1**, **L-Zn**, and **LCo-2** in detecting nitroaromatics such as 1,2-DNB (1,2-dinitrobenzene), 1,3-DNB (1,3-dinitrobenzene), CDNB (2,4-dinitrochlorobenzene), 2,4-DNPH (2,4-dinitrophenylhydrazine), 4-NA (4-nitroaniline), and 4-NP (4-nitrophenol) is tested. Fig. S1–S18 (ESI†) show incremental addition of analytes and Fig. 4(b) shows the Stern–Volmer plots for nitroaromatic compounds in

the presence of **LCo-1**. It is observed that analytes 1,2-DNB, 1,3-DNB, and CDNB showed a negligible quenching effect for photoluminescence from **LCo-1** indicating that the detection response for these analytes is nearly zero; the same compound showed a very diminutive response at higher concentrations for 2,4-DNPH. On the other hand, considerable quenching in the intensity of emission peaks were observed for 4-NA and 4-NP
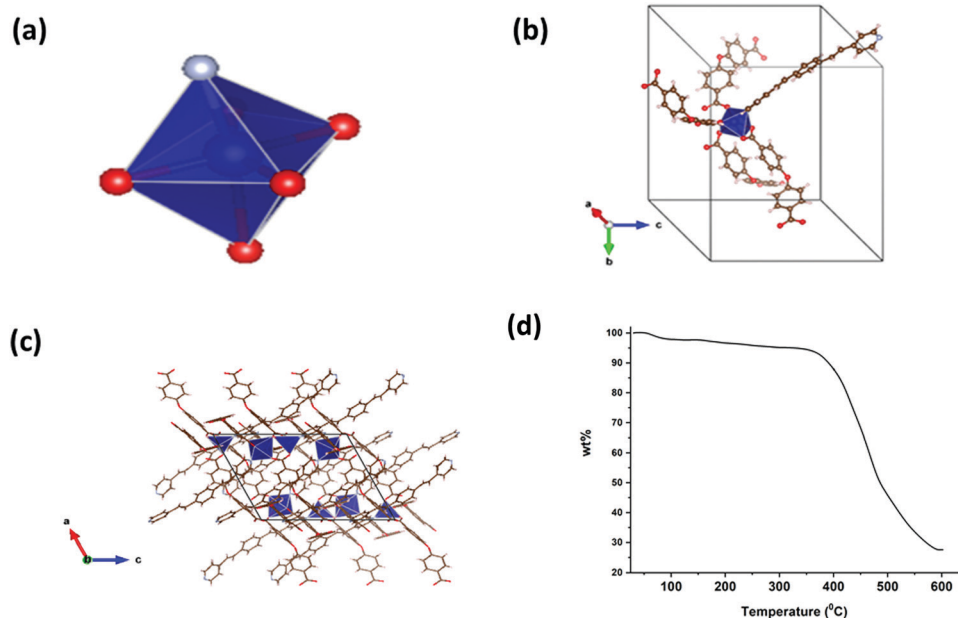
Fig. 3 (a) The SBU unit of the **LCo-2** MOF with color code blue: central atom (Co), red: oxygen atoms and indigo blue: nitrogen; (b) complete structure of the SBU with coordinating molecules bpeb and oba; (c) 3-dimensional structure, and (d) thermogravimetric curve of the **LCo-2** MOF.
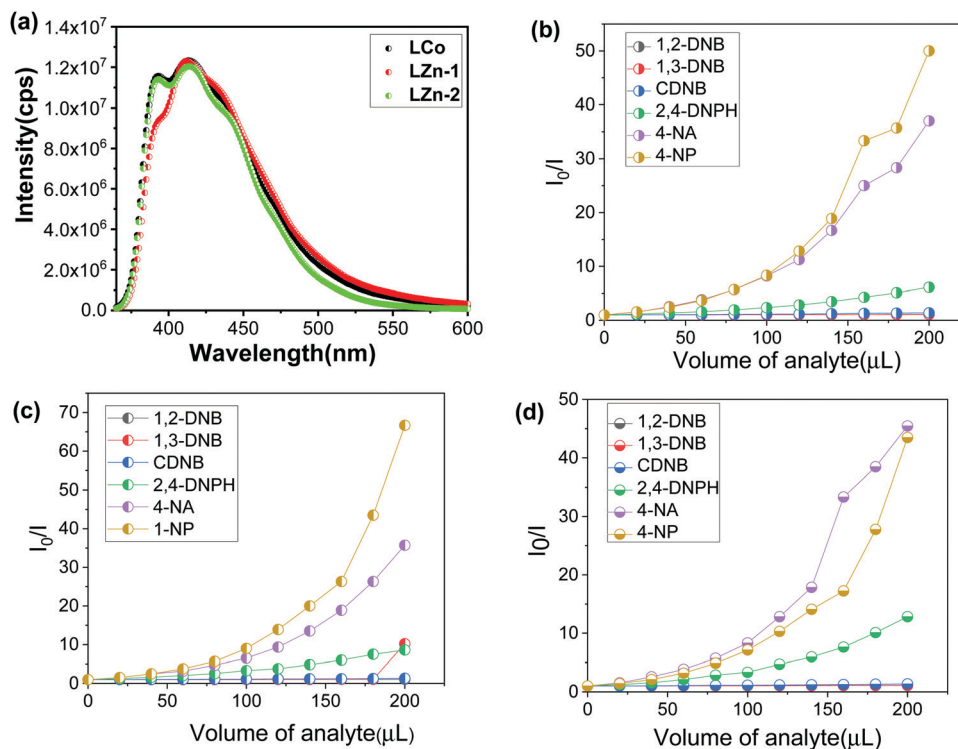

Fig. 4 (a) Fluorescence spectra of (i) **LCo-1**, (ii) **L-Zn** and (iii) **LCo-2** and (b), (c), and (d) Stern–Volmer plots of different nitroaromatic compounds with **LCo-1**, **L-Zn**, and **LCo-2** respectively.

indicating the specificity of **LCo-1** for the detection of 4-NA and 4-NP, and the quenching efficiency of these analytes varied linearly with the concentration, with quenching constant values and respectively (Fig. 4(b)). The comparative response for

different analytes towards the quenching of PL from **LCo-1** is plotted in Fig. 5(a); the results show that 4-NA and 4-NP have shown nearly 98% quenching, 2,4-DNPH showed nearly 6% and the other analytes 1,2-DNB, 1,3-DNB, and CDNB showed less
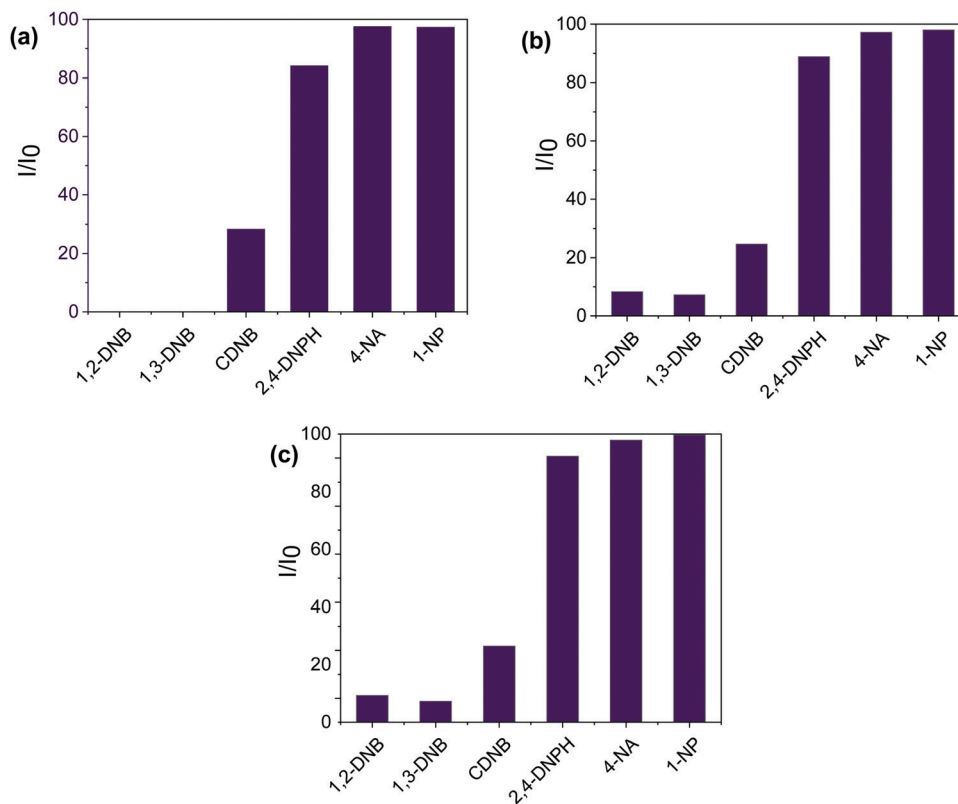
Fig. 5 PL quenching efficiency of different analytes in the presence of (a) **LCo-1**; (b) **L–Zn**; and (c) **LCo-2** respectively for 200 μL analyte volume.

than 2% indicating the selective PL response of **LCo-1** in detecting 4-NA and 4-NP. The luminescence quenching profiles of **L-Zn** and **LCo-2**, in the presence of specified analytes, are shown in Fig. 4(c) and (d). The literature reports reveal that there are only a handful of MOFs that show sensing towards one or more nitro analytes.[32] In this context, the three MOFs presented herein have the capability of detecting multiple analytes for potential applications.

fluorescence response of the MOFs in detecting 4-NA, 4-NP and 2,4-DNPH. Based on the results we conclude that the reported three MOFs have the potential to detect multiple aromatic nitro-analytes.

Conflicts of interest

The authors declare no conflict of interest.

Conclusions

In this contribution, we successfully synthesized two 2D MOFs and one 3D MOF using a mixed-ligand strategy. Compounds **1** and **2** were synthesized using the same combination of ligands but by varying the metals whereas compound **3** was synthesized by introducing the bent shaped oba ligand. The change in structural dimensionality highlights the impact of the bpeb, hfipbb, and oba linkers and diverse bridging mode of carboxylate ligands on the synthesis of luminescent MOFs. The PL studies suggest that the bpeb linker greatly contributes to showing the fluorescence behaviour in all the three MOFs as bpeb has a highly conjugated system. The fluorescence behaviour has been studied for three MOFs, **LCo-1**; **L-Zn**; and **LCo-2**, in the presence of nitro analytes and the results show that 4-NA and 4-NP have shown nearly 98% quenching, and 2,4-DNPH showed nearly 6%. The other analytes, 1,2-DNB, 1,3-DNB, and CDNB, showed less than 2% indicating the selective

References

1 (a) S. Kitagawa, R. Kitaura and S. Noro, *Angew. Chem., Int. Ed.*, 2004, **43**, 2334; (b) C. Janiak, *J. Chem. Soc., Dalton Trans.*, 2003, 2781; (c) O. M. Yaghi, M. O'Keeffe, N. W. Ockwing, H. K. Chae, M. Eddaoudi and J. Kim, *Nature*, 2003, **423**, 705; (d) D. N. Dybtsev, M. P. Yutkin, E. V. Peresypkina, A. V. Virovets, C. Serre, G. Ferey and V. P. Fedin, *Inorg. Chem.*, 2007, **46**, 6843.
2 (a) J. R. Li, J. Sculley and H. C. Zhou, *Chem. Rev.*, 2012, **112**, 869; (b) H. Furukawa, K. E. Cordova, M. O'Keeffe and O. M. Yaghi, *Science*, 2013, **341**, 974; (c) L. J. Murray, M. Dinca and J. R. Long, *Chem. Soc. Rev.*, 2009, **38**, 1294; (d) W. Yang, A. J. Davies, X. Lin, M. Suyetin, R. Matsuda, A. J. Blake, C. Wilson, W. Lewis, J. E. Parker, C. C. Tang, M. W. George, P. Hubberstey, S. Kitagawa, H. Sakamoto, E. Bichoutskaia, N. R. Champness, S. Yang and M. Schroder, *Chem. Sci.*, 2012, **3**, 2993.

3 (a) L. Ma, C. Abney and W. Lin, *Chem. Soc. Rev.*, 2009, **38**, 1248; (b) D. N. Dybtsev, A. L. Nuzhdin, H. Chun, K. P. Bryliakov, E. P. Talsi, V. P. Fedin and K. Kim, *Angew. Chem., Int. Ed.*, 2006, **45**, 916; (c) S. H. Cho, B. Ma, S. T. Nguyen, J. T. Hupp and T. E. Albrecht-Schmittb, *Chem. Commun.*, 2006, 2563.

4 (a) O. K. Farha and J. T. Hupp, *Acc. Chem. Res.*, 2010, **43**, 1166; (b) P. Horcajada, C. Serre, M. Vallet-Regi, M. Sebban, F. Taulelle and G. Ferey, *Angew. Chem., Int. Ed.*, 2006, **45**, 5974; (c) J. D. Rocca, D. Liu and W. Lin, *Acc. Chem. Res.*, 2011, **44**, 957 and references cited therein.

5 (a) L. E. Kreno, K. Leong, O. K. Farha, M. Allendorf, R. P. Van Duyne and J. T. Hupp, *Chem. Rev.*, 2012, **112**, 1105 and references cited therein ; (b) Y. Cui, Y. Yue, G. Qian and B. Chen, *Chem. Rev.*, 2012, **112**, 1126 and references cited therein.

6 (a) C. N. R. Rao, A. K. Cheetham and A. Thirumurugan, *J. Phys. Condens. Matter.*, 2008, **20**, 083202; (b) A. Chakraborty, B. K. Ghosh, J. B. Arino, J. Ribas and T. K. Maji, *Inorg. Chem.*, 2012, **51**, 6440; (c) G. J. Halder, C. J. Kepert, B. Moubaraki, K. S. Murray and J. D. Cashion, *Science*, 2002, **298**, 1762; (d) M. Kurmoo and Chem Soc, *Rev*, 2009, **38**, 1353 and reference cited therein; (e) C. Dey, R. Das, B. K. Saha, P. Poddar and R. Banerjee, *Chem. Commun.*, 2011, **47**, 11008.

7 (a) C. Dey, T. Kundu and R. Banerjee, *Chem. Commun.*, 2012, **48**, 266; (b) T. Panda, T. Kundu and R. Banerjee, *Chem. Commun.*, 2012, **48**, 5464; (c) P. K. Thallapally, J. W. Grateb and R. K. Motkuri, *Chem. Commun.*, 2012, **48**, 347; (d) S. Jin, H.-J. Son, O. K. Farha, G. P. Wiederrecht and J. T. Hupp, *J. Am. Chem. Soc.*, 2013, **135**, 955.

8 (a) M. Eddaoudi, J. Kim, N. Rosi, D. Vodak, J. Wachter, M. O'Keeffe and O. M. Yaghi, *Science*, 2002, **295**, 469; (b) M. Eddaoudi, H. L. Li and O. M. Yaghi, *J. Am. Chem. Soc.*, 2000, **122**, 1391.

9 (a) J. Seo, R. Matsuda, H. Sakamoto, C. Bonneau and S. Kitagawa, *J. Am. Chem. Soc.*, 2009, **131**, 12792; (b) I. Beurroies, M. Boulhout, P. L. Llewellyn, B. Kuchta, G. Férey, C. Serre and R. Denoyel, *Angew. Chem., Int. Ed.*, 2010, **49**, 7526; (c) M. Dan-Hardi, H. Chevreau, T. Devic, P. Horcajada, G. Maurin, G. Fédrey, D. Popov, C. Riekel, S. Wuttke, J.-C. Lavalley, A. Vimont, T. Boudewijns, D. deVos and C. Serre, *Chem. Mater.*, 2012, **24**, 2486; (d) P. K. Thallapally, J. Tian, M. Radha Kishan, C. A. Fernandez, S. J. Dalgarno, P. B. McGrail, J. E. Warren and J. L. Atwood, *J. Am. Chem. Soc*, 2008, **130**, 16842.

10 (a) K. Biradha and M. Fujita, *Angew. Chem., Int. Ed.*, 2002, **41**, 3392; (b) S. Mohapatra, H. Sato, R. Matsuda, S. Kitagawa and T. K. Maji, *CrystEngComm*, 2012, **14**, 4153; (c) T. K. Maji, G. Mostafa, R. Matsuda and S. Kitagawa, *J. Am. Chem. Soc.*, 2005, **127**, 17152.

11 (a) T. K. Kim and M. P. Suh, *Chem. Commun.*, 2011, **47**, 4258; (b) D. H. Hong and M. P. Suh, *Chem. Commun.*, 2012, **48**, 9168; (c) N. F. Sciortino, K. R. Scherl-Gruenwald, G. Chastanet, G. J. Halder, K. W. Chapman, J. F. Letard and C. J. Kepert, *Angew. Chem., Int. Ed.*, 2012, **51**, 10154;

(d) J. Zhang, H. Wu, T. J. Emge and J. Li, *Chem. Commun.*, 2010, **46**, 9152.

12 (a) B. Manna, A. K. Chaudhari, B. Joarder, A. Karmakar and S. K. Ghosh, *Angew. Chem., Int. Ed.*, 2013, **52**, 998; (b) H. B. Cui, B. Zhou, L.-S. Long, Y. Okano, H. Kobayashi and A. Kobayashi, *Angew. Chem., Int. Ed.*, 2008, **47**, 3376; (c) J. A. R. Navarro, E. Barea, A. Rodriguez-Dieguez, J. M. Salas, C. O. Ania, J. B. Parra, N. Masciocchi, S. Galli and A. Sironi, *J. Am. Chem. Soc.*, 2008, **130**, 3978.

13 (a) V. Laget, C. Hornick, P. Rabu, M. Drillon and R. Ziessel, *Coord. Chem. Rev.*, 1998, **178–180**, 1533, and references cited therein; (b) B. N. Figgis, M. Gerloch, J. Lewis, F. E. Mabbs and G. A. Webb, *J. Chem. Soc. A*, 1968, 2086; (c) M. Gerloch and P. N. Quested, *J. Chem. Soc. A*, 1971, 3729; (d) F. E. Mabbs and D. J. Machin, *Magnetism in Transition Metal Complexes*, Chapman and Hall, London, 1973; (e) C. M. Nagaraja, N. Kumar, T. K. Maji and C. N. R. Rao, *Eur. J. Inorg. Chem.*, 2011, 2057; (f) X. Y. Wang, L. Gan, S. W. Zhang and S. Gao, *Inorg. Chem.*, 2004, **43**, 4615.

14 (a) P. Kanoo, K. L. Gurunatha and T. K. Maji, *J. Mater. Chem.*, 2010, **20**, 1322; (b) K. L. Gurunatha and T. K. Maji, *Inorg. Chem.*, 2009, **48**, 10886.

15 (a) T. K. Maji, S. Pal, K. L. Gurunatha, A. Govindaraj and C. N. R. Rao, *Dalton Trans.*, 2009, 4426; (b) S. Mohapatra, H. Sato, R. Matsuda, S. Kitagawa and T. K. Maji, *CrystEngComm*, 2012, **14**, 4153; (c) S. K. Ghosh, R. Azhakar and S. Kitagawa, *Chem. Asian J.*, 2009, **4**, 870.

16 R. De Jong and M. de Puit, *Forensic Sci. Int.*, 2018, **291**, 12–16.

17 R. Kaur, A. K. Paul and A. Deep, *Forensic Sci. Int.*, 2014, **242**, 88–93, DOI: 10.1016/j.forsciint.2014.06.028.

18 F. G. M. Mauricio, A. Z. Pralon, M. Talhavini, M. O. Rodrigues and I. T. Weber, *Forensic Sci. Int.*, 2017, **275**, 8–13.

19 M.-L. Hu, S. A. A. Razavi, M. Piroozzadeh and A. Morsali, *Inorg. Chem. Front.*, 2020, **7**, 1598–1632, DOI: 10.1039/c9qi01617a.

20 A. Harshey, T. Das and A. Srivastava, *Microchem. J.*, 2020, **154**, 104597.

21 S. Moret, E. Scott, A. Barone, K. Liang, C. Lennard, C. Roux and X. Spindler, *Forensic Sci. Int.*, 2018, **291**, 83–93, DOI: 10.1016/j.forsciint.20180.8.005.

22 M. R. Hafner, F. Carraro, L. A. Brandner, S. Maniam, G. Grenci, S. L. Holzer, H. Bischof, R. Malli, S. M. Borisov, C. Doonan and P. Falcaro, *Chem. Commun.*, 2020, **56**, 12733; H. Xu, C.-S. Cao, X.-M. Kang and B. Zhao, *Dalton Transactions*, 2016, **45**, 18003–18017.

23 S.-N. Zhao, G. Wang, D. Poelman and P. Voort, *Materials*, 2018, **11**, 572.

24 S. E. Miller, M. H. Teplensky, P. Z. Moghadam and D. Fairen-Jimenez, *Interface Focus*, 2016, **6**(4), 20160027.

25 Z.-J. Lin, J. Lü, M. Hong and R. Cao, *Chem. Soc. Rev.*, 2014, **43**, 5867–5895.

26 D. Banerjee, Z. Hu and J. Li, *Dalton Trans.*, 2014, **43**, 10668–10685.

27 X. Fang, B. Zong and S. Mao, *Nano-Micro Lett.*, 2018, **10**(4), DOI: 10.1007/s40820-018-0218-0.

28 S. Khullar, S. Singh, P. Das and S. K. Mandal, *ACS Omega*, 2019, **4**, 5283–5292.

29 K.-S. Ju and R. E. Parales, *Microbiol. Mol. Biol. Rev.*, 2010, **74**(2), 250–272.

30 M. H. Priya and G. Madras, *J. Photochem. Photobiol., A*, 2016, **178**, 1–7.

31 S. H. Toma, M. Uemi, S. Nikolaou, D. M. Tomazela, M. N. Eberlin and H. E. Toma, *Inorg. Chem.*, 2004, **43**, 3521–3527.

32 Z. Hu, B. J. Deibert and J. Li, *Chem. Soc. Rev.*, 2014, **43**, 5815.